



**HAL**  
open science

# Crystal nucleation in adroplet based microfluidic crystallizer

Sébastien Teychené, Béatrice Biscans

► **To cite this version:**

Sébastien Teychené, Béatrice Biscans. Crystal nucleation in adroplet based microfluidic crystallizer. Chemical Engineering Science, 2012, 77, pp.242-248. 10.1016/J.CES.2012.01.036 . hal-03536968

**HAL Id: hal-03536968**

**<https://hal.science/hal-03536968v1>**

Submitted on 20 Jan 2022

**HAL** is a multi-disciplinary open access archive for the deposit and dissemination of scientific research documents, whether they are published or not. The documents may come from teaching and research institutions in France or abroad, or from public or private research centers.

L'archive ouverte pluridisciplinaire **HAL**, est destinée au dépôt et à la diffusion de documents scientifiques de niveau recherche, publiés ou non, émanant des établissements d'enseignement et de recherche français ou étrangers, des laboratoires publics ou privés.



## Open Archive Toulouse Archive Ouverte (OATAO)

OATAO is an open access repository that collects the work of Toulouse researchers and makes it freely available over the web where possible.

This is an author-deposited version published in: <http://oatao.univ-toulouse.fr/>  
Eprints ID: 6138

**To link to this article:** DOI:10.1016/J.CES.2012.01.036  
URL: <http://dx.doi.org/10.1016/J.CES.2012.01.036>

<p><b>To cite this version:</b> Teychené, Sébastien and Biscans, Béatrice (2012) Crystal nucleation in adroplet based microfluidic crystallizer. <i>Chemical Engineering Science</i> vol. 77. pp. 242-248. ISSN 0009-2509</p>
---

Any correspondence concerning this service should be sent to the repository administrator: [staff-oatao@listes.diff.inp-toulouse.fr](mailto:staff-oatao@listes.diff.inp-toulouse.fr)

# Crystal nucleation in a droplet based microfluidic crystallizer

S. Teychené\*, B. Biscans

Laboratoire de Génie Chimique, UMR CNRS 5503, Université de Toulouse, 4 Allée Emile Monso 31432, Toulouse, France

---

## A B S T R A C T

The study presented in this paper deals with the determination of eflucimibe nucleation rate in a droplet based microfluidic crystallizer. The experimental device allows the storage of up to 2000 monodispersed droplets to get nucleation statistics and crystal growth rates under static conditions. Supersaturation was generated by quenching the droplets down to 273 or 293 K. To determine the nucleation kinetics of eflucimibe, the number of appearing crystals is recorded as a function of time. At low time scale, it was found that eflucimibe in the droplets containing active centers (impurities) crystallizes first and thus yields a rapid initial rate. At higher time scale, once all the droplets containing impurities have crystallized, leaving only the droplets that are free of impurities, the nucleation rate falls allowing the determination of the homogeneous nucleation rate. The crystal–solution interfacial energy found in this system  $\sigma=3.12 \text{ mJ m}^{-2}$  is in good agreement with the previously published results. Using the crystal nucleation and the growth rate determined experimentally, simulations were performed using a Monte Carlo method. Even if this method correctly predicts the number of droplets that remains empty during the experiments, it was not possible to predict correctly the number of crystals per drop obtained experimentally. The relationship between the growth and nucleation rates and the resultant number of crystals per drop is likely to be complex and dependent on a number of system parameters. The failure of the model may be attributed either to an overestimation of the crystal growth rate or to an enhancement of the nucleation rate due to the presence of seed crystals.

---

## 1. Introduction

Crystallization from solution is a core technology in pharmaceutical industries. Usually, this process is a part of a wide processing system, including solid–liquid separation, particle design, and formulation. In the field of pharmaceutical industry, chemical engineers must develop a robust crystallization process that delivers the active pharmaceutical ingredient (API) with both high yield and appropriate attributes that are conducive to drug product development (e.g., purity, polymorph and particle size distribution). To reach this goal, it is essential that fundamental data on nucleation kinetics, crystal growth and phase transitions should be determined precisely. Nucleation, as a stochastic phenomenon by nature (Izmailov et al., 1999), is known to be difficult to reproduce and even experiments performed with great care may lead to a large variability (Teychené and Biscans, 2008). To work around the problem of stochasticity, several experimental techniques, mainly inspired by the work of Turnbull and Vonnegut (1952), are based on the duplication of the same experiments in a small crystallization container (droplet or microwell for instance). Among these experimental techniques, droplet based microfluidic offers the unique opportunity to control droplets in time and space. This latter technique enables to generate crystallization containers with perfectly controlled operating

conditions (Teychené and Biscans, 2011; Laval et al., 2007a; Zheng et al., 2004; Saeila et al., 2009). Recently, we have proposed a glass made microfluidic chip to study nucleation and phase transition of organic materials confined in droplets of organic solvents. In addition, at the micrometric scale the two-phases flow is only controlled by capillary and viscous forces. Thus monodispersed droplets, used as crystallization containers, can be generated without a surfactant. This point can be important when studying nucleation and crystal growth rates, as surface-active molecules can have a significant effect due to molecular similarity (Davey et al., 1997) and can favor the appearance of an undesired polymorph (Yano et al., 2000), or can alter the thermodynamic equilibrium. The main objective of this paper is to study nucleation and growth kinetics of a complex molecule, i.e. eflucimibe, in droplets of octanol generated in water without surfactant. The experimental kinetics obtained are used as an input for a Monte Carlo model to describe the temporal evolution of the number of empty drops and the number of crystals per drop within the microfluidic crystallizer.

## 2. Material and methods

### 2.1. Material

Octan-1-ol (with a minimum purity of 99.5%) was purchased from Sigma-Aldrich. The solvent was used without further

---

\* Corresponding author. Tel.: +33 534323637.

E-mail address: Sebastien.Teychene@ensiacet.fr (S. Teychené).

purification. Double distilled water was processed through a Barnstead EASY pure UV system. The water resistivity was greater than 18 M $\Omega$  cm.

Eflucimibe ((2S)-2-dodecylsulfanyl-N-(4-hydroxy-2,3,5-trimethylphenyl)-2-phenylacetamide, C<sub>29</sub>H<sub>43</sub>NO<sub>2</sub>S, M=469.73 g mol<sup>-1</sup>) was supplied by Pierre Fabre Company, Gaillac, France. Its chemical purity, evaluated by high-performance liquid chromatography, was more than 99.5%.

## 2.2. Experimental setup

The microfluidic crystallization chip consists in a droplet generator (cross geometry) and a 2.5 m long serpentine (Fig. 1a). This long serpentine, made by 64 parallel channels, is used either to allow to reach enough residence time to observe crystallization in the droplets under flow, or to store up to 2000

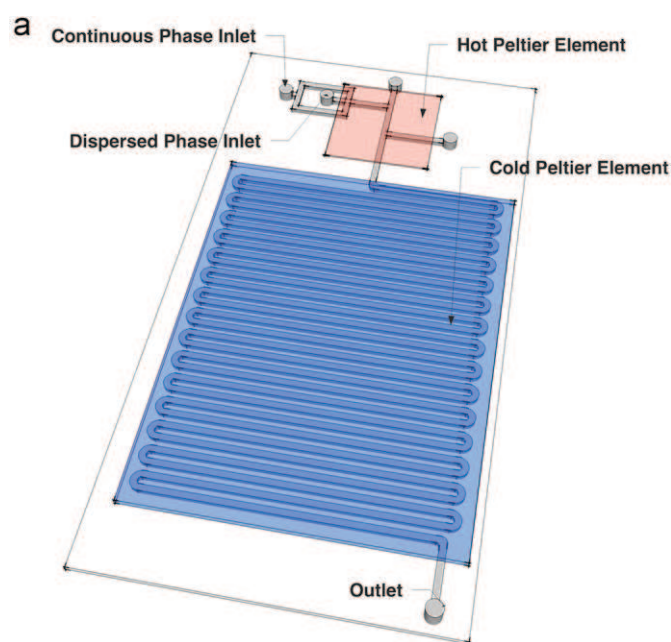


**Fig. 1.** Experimental setup. (a) sketch of the microfluidic chip and (b) the microfluidic device mounted on an inverted microscope.

**Table 1**  
Operating conditions of the crystallization experiments.

Exp. number	Initial temperature (K)	Final temperature (K)	Supersaturation, $S=C/C^*$	Mean droplet length, $L_d$ ( $\mu$ m)	Droplet volume, $V_d$ (nl)
#1	310.15	293.15	2.38	509	11.3
#2	320.15	293.15	2.80	522	11.4
#3	313.15	278.15	3.14	530	11.7
#4	323.15	278.15	4.21	517	11.4
#5	333.15	278.15	4.79	526	11.5

droplets. The chip is made of glass and was built by Micronit (Eschende, The Netherlands).

To induce crystallization by a temperature change, the chip is thermally controlled by two Peltier elements. Temperature sensors and the thermoelectric elements are coupled to a PID regulator (ALI 2420, AMS Technology). This thermal system ensures a homogeneous temperature field across the chip with an accuracy of  $\pm 0.05$  °C.

Glass syringes (Hamilton 1004 series, 2.5 ml) mounted on two syringe pumps (PHD 2200, Harvard Apparatus) are used to load the fluid into the chip with a controlled flow rate. To prevent unwanted crystallization, a flexible heater (Watlow) warms the syringe and the tubing containing the organic solution.

The system is observed under a semi-automatic inverted light microscope (Zeiss AXIO Observer, Motorized stage from Ludl Electronic Product). Images are acquired using a sensitive CCD color camera (PCO, Sensicam QE) at a fixed time interval. The complete experimental setup is shown in Fig. 1b.

A more complete description of the experimental setup and of the droplet generation can be found in a previously published paper (Teychené and Biscans, 2011).

## 2.3. Crystallization procedure

First, thousands of monodispersed organic solution droplet are generated in water, 5 °C above the saturation temperature. In microfluidic systems, the droplet's diameter is usually controlled by altering the flow rate of the continuous and dispersed phases, respectively. In this study, the flow rates were fixed to 500  $\mu$ l/h for water and to 200  $\mu$ l/h for the organic solution. The length of the generated droplet is 520  $\mu$ m which corresponds to a crystallization volume of 11 nl.

When a steady flow is reached (typically after 10 min), the flow is stopped and the system is quickly cooled down (in less than 1 min) to the experiment temperature. During cooling, the system is allowed to equilibrate at the atmospheric pressure. Then, the inlets and outlets are closed. This procedure is performed to prevent droplet coalescence during the experiments. Once the final temperature is reached and the droplet stopped, images of the whole serpentine are acquired every 5 min to observe crystallization.

An image treatment computer program was written in Matlab to detect and to determine the properties (size, surface area, position, etc.) of the channels, the droplets, and the crystals. The detection of the crystals is based on their birefringence properties.

The experimental operation conditions explored in this study are given in Table 1.

## 3. Results and discussion

### 3.1. Nucleation frequencies determination

To determine nucleation kinetics, up to 1500 eflucimibe-octanol droplets were generated at a given supersaturation. The

droplets were stored and cooled down in the microfluidic chip, as explained above. The number of empty droplets and the number of droplets containing crystals as a function of time gives information about the nucleation frequency. The temporal evolution of the probability of finding no crystal in a droplet is given in Fig. 2a.

This probability is defined as the ratio between the number of empty droplets and the total number of droplets ( $P_0 = N_0/N_t$ ). Obviously, the probability of finding one or more crystals per drop is  $P = 1 - P_0$ . In the case of a purely homogeneous nucleation process, occurring at a rate  $J$ , the temporal evolution of the fraction of droplets containing no crystal is expected to follow a homogeneous Poisson distribution; i.e.  $\ln P_0 = -Jt$ ,  $V$  being the droplet volume. However, the plot of  $\ln P_0$  vs. time, given in Fig. 1b, is not linear. One possible explanation to the lack of linearity is the presence of active centers (impurities for instance)

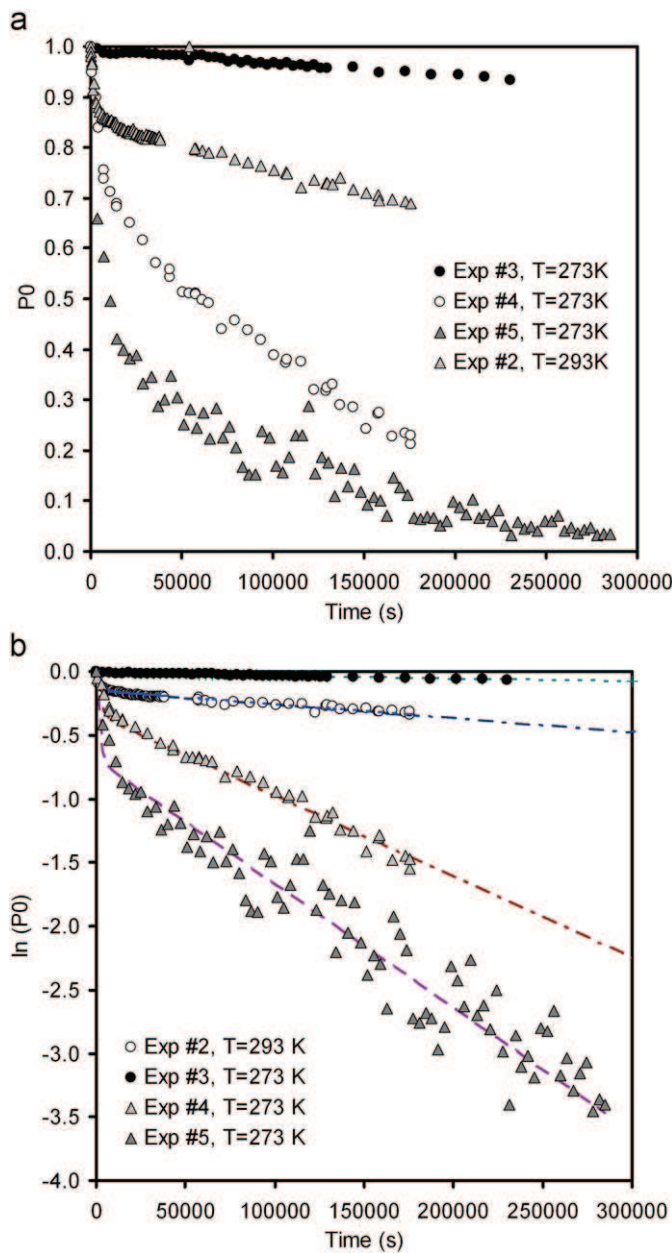


**Fig. 2.** Evolution of the nucleation probability of efflucimibe in octanol droplet. (a) ratio of empty droplet ( $P_0$ ) vs. time and (b) evolution of  $\ln(P_0)$  vs. time. The dashed lines correspond to the model of Pound and LaMer.

in the droplet which promote heterogeneous nucleation (Pound and LaMer, 1952; Laval et al., 2007b; Teychené and Biscans, 2011). Following the work of Pound and LaMer, assuming that the active centers are randomly distributed among the droplets, and that the Poisson distribution function is applicable to that distribution, the number of empty droplets containing active centers, at time  $t$ , is

$$N = N_0 \sum_{p=1}^{\infty} \frac{m^p e^{-m}}{p!} e^{-pkt} \quad (1)$$

In the same way, the number of empty droplets free from impurities is

$$N = N_0 e^{-m} e^{-k_0 t} \quad (2)$$

Accordingly, the total number of empty droplets, at time  $t$ , is

$$\begin{aligned} \ln P_0 &= \frac{N}{N_0} = e^{-m} e^{-k_0 t} + \sum_{p=1}^{\infty} \frac{m^p e^{-m}}{p!} e^{-pkt} \\ &= e^{-m} (e^{-k_0 t} - 1) + e^{-m} \exp(m e^{-kt}) \end{aligned} \quad (3)$$

where  $m$  is the arithmetic average number of active centers per droplet,  $k_0$  is the homogeneous nucleation rate and  $k$  is the heterogeneous nucleation rate. Eq. (3) was used to fit the experimental data. Typical results of the fitting are shown in Fig. 2b. It is seen that a reasonably good fit is obtained. The values obtained from the model for the nucleation rates and for the average number of active centers per droplet are given in Table 2.

In the classical nucleation theory, the rate of homogeneous nucleation, which accounts for the formation rate of critical nuclei, is related to the temperature and supersaturation by the following expression:

$$k_0 = A_0 \exp\left(-\frac{16\pi\sigma^3 v_m^2}{3(kT)^3 \ln^2 S}\right) \quad (4)$$

where  $\sigma$  is the crystal-solution interfacial tension,  $v_m$  is the molecular volume of the crystallizing molecule.  $A_0$  is a pre-exponential factor that accounts for the attachment frequency of the molecules to the emerging cluster, and  $S$  the supersaturation ratio ( $S = C/C^*$ ). The evolution of the homogeneous nucleation rate,  $k_0$ , obtained from Pound and LaMer equation, as a function of  $T^{-3} \ln^{-2}(S)$  is plotted in Fig. 3. A linear fit allows to determine the crystal solution interfacial tension  $\sigma = 3.12 \text{ mJ m}^{-2}$ , assuming a molecular volume of efflucimibe  $v_m = 4.3 \times 10^{-28} \text{ m}^3$ .

Fig. 3 also shows the evolution of the heterogeneous nucleation rate as function of  $T^{-3} \ln^{-2} S$ . As expected, the evolution of the heterogeneous nucleation rate is less influenced by supersaturation and temperature than the homogeneous nucleation rate. However the results for heterogeneous nucleation are more subtle to interpret with the model. As shown in Fig. 4, the average number of active centers in the droplet shows a significant increase with the initial temperature.

**Table 2**

Results obtained from the Pound and LaMer model for the homogeneous and heterogeneous nucleation rates ( $k_0$  and  $k$ , respectively), the average number of active centers ( $m$ ) and the Root Mean Square Error of the fit (RMSE).

Experiment number	$k_0$ ( $\text{s}^{-1}$ )	$k$ ( $\text{s}^{-1}$ )	$m$	RMSE*
1	$7.18 \times 10^{-8}$	$3.26 \times 10^{-4}$	0.008	0.11
2	$1.28 \times 10^{-6}$	$4.27 \times 10^{-4}$	0.144	0.13
3	$2.58 \times 10^{-6}$	$4.10 \times 10^{-4}$	0.011	0.15
4	$6.74 \times 10^{-6}$	$5.18 \times 10^{-4}$	0.296	0.09
5	$8.60 \times 10^{-6}$	$4.08 \times 10^{-4}$	0.694	0.11

$$* \text{RMSE} = \sqrt{\frac{1}{M} \sum_{i=1}^M |(\ln P_0)_i^{\text{ex}} - (\ln P_0)_i^{\text{pred}}|^2}$$

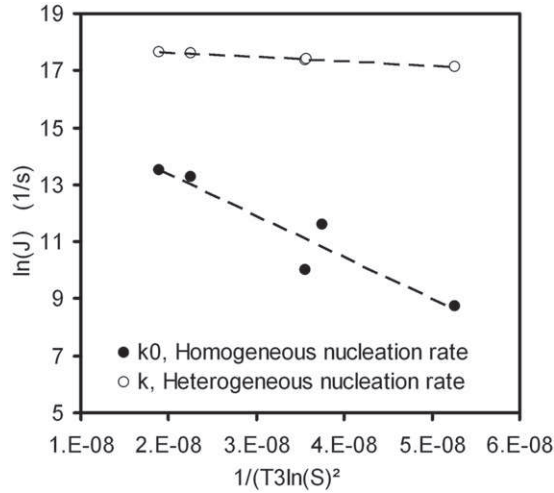


**Fig. 3.** Evolution of the heterogeneous ( $k$ ) and homogeneous ( $k_0$ ) nucleation rates with  $1/T^3 \ln(S)^2$ .

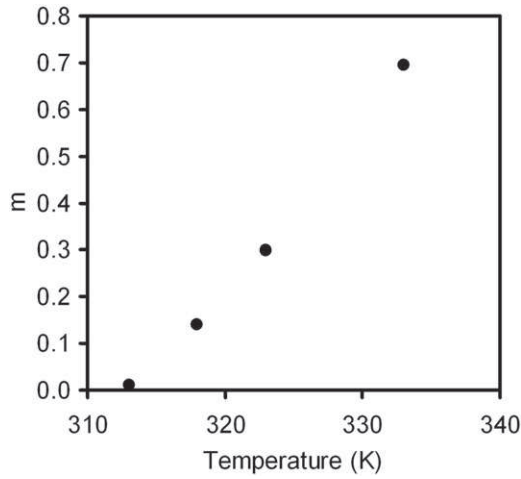


**Fig. 4.** Evolution of the average number of active centers (impurities) in the droplet ( $m$ ) with the initial temperature.

As already pointed out by numerous authors (Pound and LaMer, 1952; Turnbull and Vonnegut, 1952), at a given temperature all active centers are not equally effective as nucleating agents. This results in a variability of the number and concentration of nucleating agents in the droplet. Indeed, foreign nuclei active at a given temperature should still be effective (even more) at lower temperature, so that the heterogeneous nucleation rate measured at low temperature can be the results of both nucleation agents active at lower and higher temperatures. Consequently, as the number of active centers and their activity changes during measurements, the obtained heterogeneous nucleation rate is probably a mean value of several types of nuclei.

### 3.2. Crystal growth rate measurements

Crystal growth rate measurements were performed by following the time evolution of a crystal in 6–15 droplets for each experiment. Note that the smallest crystal size detectable is given by the camera spatial resolution and the microscope objective used. In our case, the microscope was used with a  $5\times$  or  $10\times$  objective and the camera resolution is  $1024 \times 1600$  pixels. Standard calibration grid was used to calibrate the microscope, and a

resolution of  $2.5 \text{ pixel}/\mu\text{m}$  and  $1.2 \text{ pixel}/\mu\text{m}$  can be reached with the  $5\times$  and  $10\times$  objectives, respectively. As 2–4 pixels are needed to detect a crystal, the minimum crystal size detectable with the experimental setup varies from 5 to  $10 \mu\text{m}$ , depending on the objectives used.

Temporal evolution of the spherulites diameters are given in Fig. 5a and b for the experiments performed at  $5^\circ\text{C}$  and  $20^\circ\text{C}$  respectively.

These figures clearly show that, for the same operating conditions (i.e. the same supersaturation and temperature), crystals in each droplet grow at the same rate. In addition, whatever the operating conditions are, the radial evolution of the spherulites scale with  $\sim t^{1/2}$ , characteristic of a diffusion limited growth (Granasy et al., 2005).

Assuming that at the end of the experiments the system has reached the thermodynamic equilibrium, and knowing the density of eflucimibe crystals determined by helium picnometry ( $\rho_c = 1120 \text{ kg/m}^3$ ), the maximum size of the spherulites can be computed from a simple mass balance:

$$d_{max} = \left[ \frac{6(C^* - C^0)}{\pi \rho_c \rho_{oct} V_{drop}} \right]^{1/3} \quad (5)$$

where  $C^*$  and  $C^0$  are the saturation and initial concentrations, respectively, and  $V_{drop}$  is the droplet volume. The theoretical and the experimental (obtained from image analysis) maximum diameters are given in Table 3.

The void fractions of the spherulites presented in Table 3 suggest that the crystals obtained at 278 K and 293 K do not have

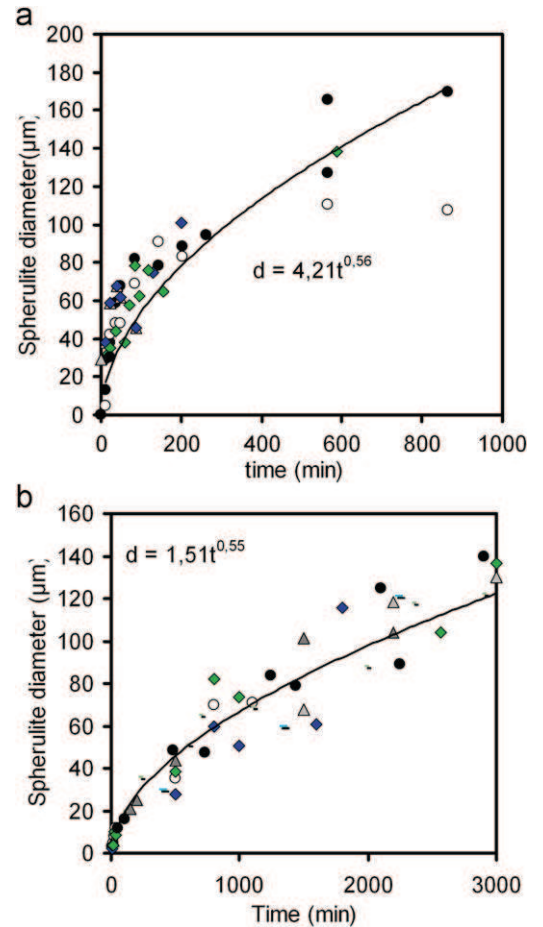


**Fig. 5.** Typical evolution of the spherulite diameters (a) Exp #5,  $T=273 \text{ K}$  and (b) Exp #2,  $T=293 \text{ K}$ .

**Table 3**  
Comparison between the maximum spherulite diameter and the measured diameter.

$T$ (K)	$S=C/C^*$	$d_{max}$ ( $\mu\text{m}$ )	$d_{mes}$ ( $\mu\text{m}$ )	$1-\varepsilon = V_{max}/V_{spherul}$
278	3.14	102	104 ( $\pm 10$ )	$\sim 1$
278	4.21	117	119 ( $\pm 11$ )	$\sim 1$
278	4.79	125	126 ( $\pm 9$ )	$\sim 1$
293	2.38	93	134 ( $\pm 16$ )	$\sim 0.3$
293	2.84			$\sim 0.3$

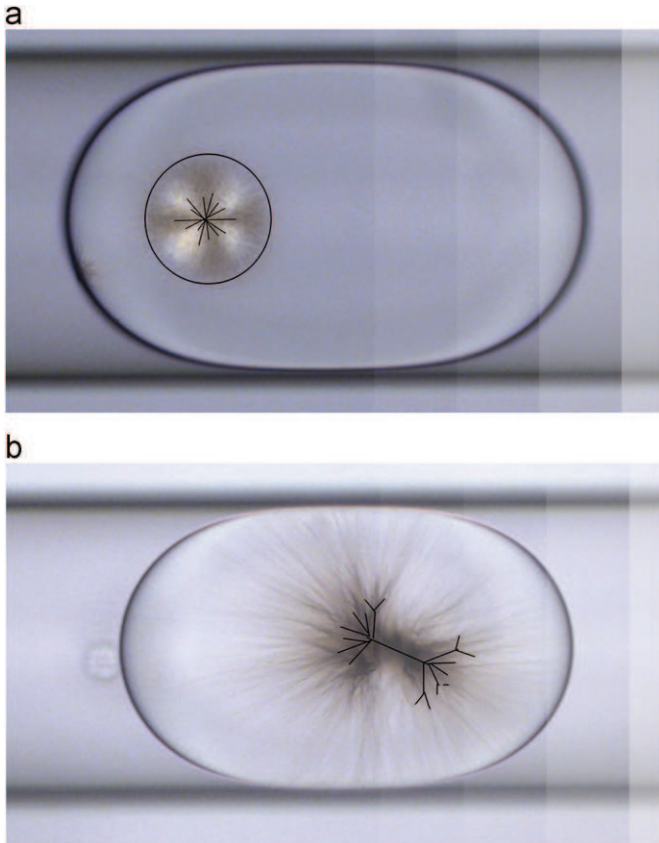


**Fig. 6.** Photograph of the spherulitic crystals obtained at (a) 278 K and (b) 293 K.

the same structure. As shown in Fig. 6, the crystals obtained at 278 K (Fig. 6a) have a much denser structure than those obtained at 293 K (Fig. 6b). Following the classification of Grànàsy et al., the crystals obtained at 278 K belong to category 1 of spherulites in which crystals are formed via central multidirectional growth. In that case, spherulites grow radially from the nucleation site, branching intermittently to maintain a nearly spherical shape. On the contrary, a second type of spherulite is obtained at 298 K. In that case, spherulites grow initially as thread-like fibers, subsequently forming new grains at the growth front. This branching of the crystallization pattern ultimately leads to a crystal ‘sheaf’ that increasingly splays out during growth. This behavior has already been observed qualitatively in a previous study (Teychené and Biscans, 2011). However, due to the complexity of spherulitic crystal formation, the origin of this change in crystal growth is still unknown, it might be due, either to a change in the crystal growth or nucleation (nucleation from liquid–liquid phase separation, for instance) mechanism with temperature or to polymorphism.

For engineering purpose, assuming that only one crystal grows in a droplet in an isotropically manner (i.e. the void fraction of the

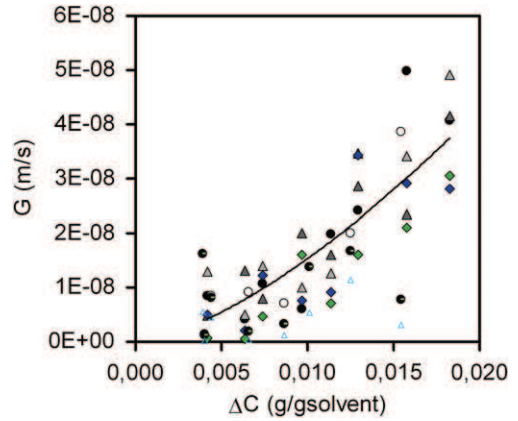


**Fig. 7.** Evolution of the crystal growth rate with the concentration driving force  $\Delta C$ .

crystal is constant during growth), the evolution of the crystal size was fitted vs. the overall concentration driving force by the general equation of crystallization:

$$G = \frac{dL}{dt} = K_G (C - C^*)^g \quad (6)$$

The result of the fitting obtained at 278 K is plotted in Fig. 7 and gives  $K_G = 1.48 \times 10^{-5} \text{ m/s(mg/g)}^{-1.5}$  and  $g = 1.5$ . However, supersaturation may also be relieved through nucleation and growth of another crystal in the droplet, provided that the concentration remains above the nucleation threshold. The relationship between the growth and nucleation rates and the resultant number of crystals per drop is likely to be complex and dependent of a number of system parameters. Simplified model such as population balance or Monte Carlo, can provide some insight into the expected impact of the important process parameters.

### 3.3. Monte Carlo simulation of eflocimibe crystallization

Monte Carlo models are convenient tools for dealing with random processes by repeated sampling to obtain a representation of the system. As observed experimentally, a droplet could contain more than one crystal per drop. The decrease in the nucleation rate as a crystal grows presents some low probability events in the population balance model, since it is highly unlikely, but still theoretically possible, for a second, and a third, crystal to nucleate when the concentration is just above the nucleation threshold. Monte Carlo methods are an efficient way to simulate complex, multivariate systems, such as multiple crystals in droplets, since very low probability outcomes do not enter effectively into the computation (Ramkrishna, 2000). In that way, Dombrowski et al. 2007 have developed a Monte Carlo method for the simulation of homogeneous nucleation and growth of  $\alpha$ -lactose crystals in water droplets. In this study, the authors have shown that the prediction of the population balance and Monte Carlo models are consistent with each other and with the analytical solutions.

As shown in Fig. 2b, the rate at which a droplet remains without any crystal is not constant. Accordingly, the lack of linearity in the plot shown in Fig. 2b suggests that this nucleation phenomenon can be described by a non-homogeneous Poisson process. A non-homogeneous Poisson process is defined as a homogeneous Poisson process with a time dependence intensity  $\lambda(t)$ :

$$m(t) = \int_0^t \lambda(x) dx \quad (7)$$

$$P((N(t+dt)-N(t)=n) = \frac{e^{-(m(t+dt)-m(t))} (m(t+dt)-m(t))^n}{n!} \quad (8)$$

According to Eq. (3), the change in the rate at which the droplets remains empty during the time  $dt$  is defined as

$$m(t+dt)-m(t) = \frac{d \ln P_0}{dt} \quad (9)$$

thus, the probability that a droplet remains empty during, the time  $dt$ , is given by

$$P((N(t+dt)-N(t)=0) = e^{-(m(t+dt)-m(t))} = e^{-(d \ln P_0/dt)} \quad (10)$$

The entire structure and assumptions of the Monte Carlo method can be found by Dombrowsky et al. (2007). For the sake of clarity, this method can be summarized as follows:

- 1- A random number is drawn from an uniform distribution.
- 2- The random number is compared to the nucleation probability. Since the chance of drawing a number less than the nucleation probability is equal to that probability, if the number is less than the nucleation probability, a new crystal nucleate.
- 3- Then crystals grow according to Eq. (6).
- 4- The new supersaturation, and the corresponding nucleation and growth rates are calculated and the simulation returns to point 1.
- 5- If nucleation failed, any existing crystals grow and all the parameters are calculated.

This process is repeated until the simulation time is reached for all the droplets (10,000). It was found that for a time step less than 50 s the deviation is less than 2% between simulations. The outputs of the model are the total number of crystals per droplet and the crystal size distribution.

The Monte Carlo simulation results obtained in terms of probability of finding no crystals in the droplet as a function of time and corresponding experiments performed at  $S=2.80$  ( $T=293$  K) and  $S=4.79$  ( $T=278$  K) are plotted in Fig. 8a and b, respectively. This figure clearly shows that the Monte Carlo simulation results are in really good agreement with the experiments. The two nucleation kinetics found experimentally are well described. This method can be very useful for designing new experiments to reach, for instance, the desired amount of crystallized droplets or to get the mean induction time at a given operating condition.

The simulation and experimental results obtained in terms of number of crystal per drop are also plotted in Fig. 8. This figure shows that, in the case where significant amount of crystals nucleate inside the droplet, this approach greatly underestimates the number of crystals per drop. One possible explanation of this failure can be attributed to the experimentally determined crystal growth. Indeed, a too fast crystal growth kinetics can consume supersaturation too quickly, lowering the nucleation probability. To rule out a possible implication of the crystal growth kinetics, some simulations were performed by dividing the crystal growth rate by  $10^6$ , to simulate a very slow crystal growth rate. Unfortunately, the results were not acceptable. The other possible explanation of such a high number of crystals per drop found experimentally is the increase of the nucleation rate when a crystal is present in the droplet. The existing crystals in the droplet could act as a seed for the next nucleating crystals, leading to an increase of the nucleation rate. Unfortunately, with the current experimental setup, it was not possible to measure the secondary nucleation rate.

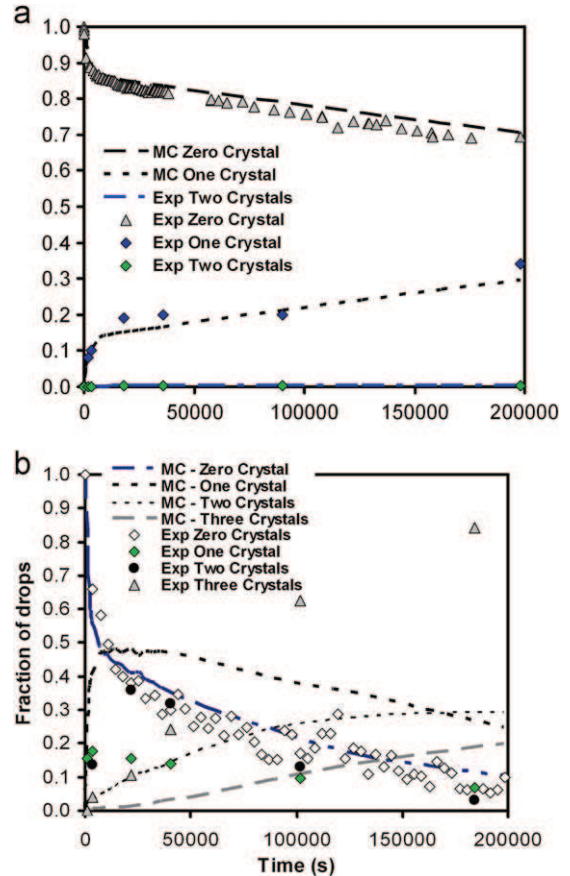


Fig. 8. Comparison between the Monte Carlo simulation and the experiments of the fractions of empty droplets, droplets containing one, two and three crystals. (a) Exp #2,  $T=298$  K and (b) Exp #5,  $T=278$  K.

#### 4. Conclusion

In this paper, eflucimibe nucleation was studied in a droplet microfluidic crystallizer. In this experimental setup, it was found that eflucimibe nucleation is firstly due to a heterogeneous nucleation process followed by a homogeneous nucleation process, when all the droplets containing the active centers have been crystallized. This experimental setup also gives the information about the spherulitic crystal growth of eflucimibe. Different mechanisms of crystal nucleation and growth were suspected at 278 K and 293 K that were responsible for the difference in the structure and density of the spherulites. Finally, a simulation model, based on the Monte Carlo simulation, was proposed to describe nucleation and growth inside the droplet. Thanks to this approach, it is possible to predict the evolution of the number of empty drops as a function of time. The fact that the model fails to predict the correct number of crystals per drop (greater than 1), whatever the crystal growth rate is, indicates that a secondary nucleation seems to be responsible for the large number of crystals obtained experimentally.

#### Acknowledgments

The author would like to thank Lucie Vialaret for her help in the experimental part. The author would also like to thank the CNRS,

the MRCT and the ANR (ANR Microcristal Project 06-BLAN-0355) for their financial support.

## References

- Davey, R.J., Hilton, A.M., Garside, J., 1997. Crystallization from oil-in-water emulsions: particle synthesis and purification of molecular materials. *Chem. Eng. Res. Des.* 75, 245–251.
- Dombrowski, R.D., Litster, J.D., Wagner, N.J., He, Y., 2007. Crystallization of alpha-lactose monohydrate in a drop-based microfluidic crystallizer. *Chem. Eng. Sci.* 62 (17), 4802–4810.
- Granasy, L., Pusztai, T., Tegze, G., Warren, J.A., Douglas, J.F., 2005. Growth and form of spherulites. *Phys. Rev. E* 72 (1), 011605.
- Izmailov, A.F., Myerson, A.S., Arnold, S., 1999. A statistical understanding of nucleation. *J. Cryst. Growth* 196 (2–4), 234–242.
- Laval, P., Lisai, N., Salmon, J.-B., Joanicot, M., 2007a. A microfluidic device based on droplet storage for screening solubility diagrams. *Lab Chip* 7 (7), 829–834.
- Laval, P., Salmon, J.-B., Joanicot, M., 2007b. A microfluidic device for investigating crystal nucleation kinetics. *J. Cryst. Growth* 303 (2), 622–628.
- Pound, G.M., LaMer, V.K., 1952. Kinetics of crystalline nucleus formation in supercooled liquid Tin<sub>1.2</sub>. *J. Am. Chem. Soc.* 74 (9), 2323–2332.
- Ramkrishna, D., 2000. *Population Balances: Theory and Applications to Particulate Systems in Engineering*. Academic Press.
- Saeila, S., Jia, Y., Fraden, S., 2009. Measuring the nucleation rate of lysozyme using microfluidics. *Cryst. Growth Des.* 9 (4), 1806–1810.
- Teychené, S., Biscans, B., 2008. Nucleation kinetics of polymorphs: induction period and interfacial energy measurements. *Cryst. Growth Des.* 8 (4), 1133–1139.
- Teychené, S., Biscans, B., 2011. Microfluidic device for the crystallization of organic molecules in organic solvents. *Cryst. Growth Des.* 11 (11), 4810–4818.
- Turnbull, D., Vonnegut, B., 1952. Nucleation catalysis. *Ind. Eng. Chem.* 44 (6), 1292–1298.
- Yano, J., Furedi-Milhofer, H., Wachtel, E., Garti, N., 2000. Crystallization of organic compounds in reversed micelles. II. Crystallization of glycine and L-phenylalanine in water-isooctane-AOT microemulsions. *Langmuir* 16, 1005–10014.
- Zheng, B., Tice, J.D., Roach, L.S., Ismagilov, R.F., 2004. A droplet-based, composite PDMS/glass capillary microfluidic system for evaluating protein crystallization conditions by microbatch and vapor-diffusion methods with on-chip X-ray diffraction. *Angew. Chem.* 116 (19), 2562–2565.